Published in final edited form as:
Magn Reson Med. 2013 July ; 70(1): 33–39. doi:10.1002/mrm.24434.

Evaluation of Heterogeneous Metabolic Profile in an Orthotopic Human Glioblastoma Xenograft Model Using Compressed Sensing Hyperpolarized 3D ^{13}C Magnetic Resonance Spectroscopic Imaging

Ilwoo Park[1,*], **Simon Hu**[1], **Robert Bok**[1], **Tomoko Ozawa**[2], **Motokazu Ito**[2], **Joydeep Mukherjee**[2], **Joanna J. Phillips**[2], **C. David James**[2], **Russell O. Pieper**[2], **Sabrina M. Ronen**[1], **Daniel B. Vigneron**[1,3], and **Sarah J. Nelson**[1,3]

[1]Department of Radiology and Biomedical Imaging, Surbeck Laboratory of Advanced Imaging, University of California, San Francisco, California, USA.

[2]Department of Neurological Surgery, Brain Tumor Research Center, University of California, San Francisco, California, USA.

[3]Department of Bioengineering and Therapeutic Sciences, University of California, San Francisco, California, USA.

Abstract

High resolution compressed sensing hyperpolarized ^{13}C magnetic resonance spectroscopic imaging was applied in orthotopic human glioblastoma xenografts for quantitative assessment of spatial variations in ^{13}C metabolic profiles and comparison with histopathology. A new compressed sensing sampling design with a factor of 3.72 acceleration was implemented to enable a factor of 4 increase in spatial resolution. Compressed sensing 3D ^{13}C magnetic resonance spectroscopic imaging data were acquired from a phantom and 10 tumor-bearing rats following injection of hyperpolarized [1-^{13}C]-pyruvate using a 3T scanner. The ^{13}C metabolic profiles were compared with hematoxylin and eosin staining and carbonic anhydrase 9 staining. The high-resolution compressed sensing ^{13}C magnetic resonance spectroscopic imaging data enabled the differentiation of distinct ^{13}C metabolite patterns within abnormal tissues with high specificity in similar scan times compared to the fully sampled method. The results from pathology confirmed the different characteristics of ^{13}C metabolic profiles between viable, non-necrotic, nonhypoxic tumor, and necrotic, hypoxic tissue.

Keywords

hyperpolarized ^{13}C MRSI; compressed sensing; dynamic nuclear polarization; pyruvate; glioblastoma

Dynamic nuclear polarization and the recent development of a dissolution process that retains polarization in liquid state have allowed for the acquisition of ^{13}C magnetic resonance spectroscopic imaging (MRSI) data with a substantial gain in sensitivity over conventional MR methods (1).

[*]Correspondence to: Ilwoo Park, Ph.D., 1700 4th Street, Room BH-303, San Francisco, CA 94158. Ilwoo.Park@ucsf.edu.

Recent studies using hyperpolarized [1-^{13}C]-pyruvate as a substrate have demonstrated the promise of this technique for examining in vivo tumor metabolism in brain tumors (2–4). These preclinical studies have shown the feasibility of using this technique for differentiating tumor from normal brain tissue and detecting an early response to treatment in animal models of high-grade gliomas. The further refinement of ^{13}C MRSI acquisition techniques with higher spatial resolution is of interest for assessing spatial variations in tissue metabolism due to the infiltrative nature and molecular heterogeneity of gliomas.

One of the major obstacles in acquiring hyperpolarized ^{13}C signal is the time limitation imposed by the T_1 decay of hyperpolarized compound. In order to more efficiently sample the rapidly decaying ^{13}C signal, fast imaging techniques, such as compressed sensing, have been incorporated in the acquisition of hyperpolarized ^{13}C data (5). By taking advantage of the sparsity in hyperpolarized ^{13}C spectra and the undersampling of spectral k-space, the compressed sensing technique has enabled the acquisition of hyperpolarized ^{13}C metabolites with high temporal and spatial resolution in preclinical studies involving transgenic prostate cancer and liver cancer murine models (5,6).

The purpose of this project was to implement a compressed sensing scheme tailored to the rat brain morphology and to demonstrate the utility of this method in obtaining hyperpolarized ^{13}C MRSI data for evaluating heterogeneous ^{13}C metabolic profiles within brain tumor tissue using an orthotopic human glioblastoma (GBM) xenograft model. The new compressed sensing sampling scheme was validated through phantom experiments and by comparing with fully sampled ^{13}C 3D MRSI data. Our emphasis was to quantitatively assess the compressed sensing hyperpolarized ^{13}C MRSI data and to compare ^{13}C metabolic profiles from different regions of tumor with the results from histology and immunohistochemistry.

METHODS

Design of Compressed Sensing Scheme

The compressed sensing scheme tailored to rat brain was based on a previously developed framework (5). First, an in-plane matrix size of 20 × 16 was selected based on the rat brain morphology. Then an undersampling pattern was generated in order to achieve an acceleration sufficient to cover this matrix within a reasonable acquisition time. Figure 1a shows the undersampling pattern design for the 20 × 16 in-plane matrix. Note that gradient blips were placed during the rewind portions of the flyback readout to undersample a 20 × 16 × 59 region of k_x-k_y-k_f space and k_z is fully sampled (Fig. 1b; 5). The central portion of k-space was fully sampled in order to enhance the stability of the compressed sensing reconstruction, which in this case, as shown in Figure 1a, is a 6 × 4 region of k_x-k_y space. The fractional values in Figure 1a show the sampling factors for different regions of k_x-k_y-k_f space. For example, 1/6 corresponds to a 3 × 2 × 59 block of k_x-k_y-k_f space undersampled by a factor of 6, i.e., covered after one excitation. Note that some of the 1/4 sampling regions are 2 × 2 × 59 k_x-k_y-k_f space blocks and some are 1 × 4 × 59 k_x-k_y-k_f space blocks in order to tile all the regions together into a 20 × 16 × 59 k_x-k_y-k_f space whole. As shown in Figure 1a, there are 86 k-space blocks, thus 86 phase encodes are used to cover a 20 × 16 phase encoding matrix, corresponding to a factor of (20 × 16)/86 = 3.72 acceleration. Hu et al. has explored the limits of undersampling and the effect of noise on the compressed sensing nonlinear reconstruction (5). According to the simulated data from this study, the factor of 3.72 acceleration would produce practically perfect reconstruction of compressed sensing spectra. With this acceleration, spatial resolution can be doubled in x and y while keeping scan time approximately constant.

Phantom Data Acquisition

All experiments were performed using a 3T GE Signa™ scanner (GE Healthcare, Milwaukee, WI) equipped with the multinuclear spectroscopy hardware package and a dual-tuned ^{1}H ^{13}C coil (7). In order to validate the new compressed sensing sampling pattern, a spherical phantom containing enriched [1-^{13}C]-acetate was scanned using the rat brain customized compressed sensing and fully sampled ^{13}C 3D MRSI sequences in consecutive scans. A double spin echo (echo time/pulse repetition time = 140/1000 ms) and flyback echo-planar readout on the z-axis (Fig. 1b; 8) were also incorporated.

Animal Preparation

Two different human GBM cell lines, U87 ($n = 5$) and G55 ($n = 5$), were used for creating orthotopic GBM models in 10 six-week-old male athymic rats (rnu/rnu, homozygous) purchased from Harlan (Indianapolis, IN). The details of cell culture and intracerebral implantation have been described previously (2,3). Animal studies were approved by the Institutional Animal Care and Use Committee at our institution.

^{1}H MRI

During each imaging experiment, the rat was placed on a heated pad positioned in the radiofrequency coil in the MR scanner. Anesthesia was maintained with a constant delivery of isoflurane (1–2%). Prior to each ^{13}C imaging study, high-resolution T_2-weighted anatomical images were obtained in the axial plane using a fast spin-echo sequence (echo time/pulse repetition time = 60/4000 ms, 8 cm field of view, 192 × 192 matrix, 1.5 mm slice thickness, and 8 NEX). At the completion of ^{13}C imaging, axial images were obtained using a T_1-weighted spin-echo sequence (echo time/pulse repetition time = 10/700 ms, 8 cm field of view, 320 × 192 matrix, 1.2 mm slice thickness, and 6 NEX) after the injection of 0.1 mL Gadolinium (Gd)-diethylenetriaminepentaacetic acid (DTPA) (approximately 0.2 mmol/kg).

Polarization Procedure

A mixture of 35 μL (approximately 45 mg) [1-^{13}C]-pyruvate (Isotec, Miamisburg, OH) and 15 mM OX63 trityl radical, along with 1.5 mM of Dotarem gadolinium was hyperpolarized using a HyperSense® dynamic nuclear polarization polarizer (Oxford Instruments, Abingdon, UK) at 3.35 T and 1.4°K by irradiation with 94.1 GHz microwaves using methods described previously (1). After approximately 60 min of microwave irradiation, the hyperpolarized pyruvic acid was rapidly dissolved in a saline solution with 5.96 g/L Tris (40 mM), 4.00 g/L NaOH (100 mM), and 0.1 mg/L Na_2 ethylenediaminetetraacetic acid. The final dissolved solution had a concentration of 100 mM pyruvate and pH ~7.5.

Compressed Sensing and Fully Sampled ^{13}C MRSI

Both compressed sensing and fully sampled ^{13}C 3D MRSI data were acquired using a double spin echo sequence (echo time/pulse repetition time = 140/215 ms) with centric k-space encoding, a variable flip angle scheme and flyback echo-planar readout on the z-axis (Fig. 1b) (8,9) at 20 s from the start of the injection of approximately 2.5 mL hyperpolarized [1-^{13}C]-pyruvate through the tail vein. The injection started ~10 s after dissolution and lasted 10 s. For the compressed sensing acquisition, 86 phase encodes were collected from a 20 × 16 matrix in 18.5 s, resulting in 2 × 2 × 5.4 mm resolution. For the fully sampled acquisition, 80 phase encodes were collected from a 10 × 8 matrix in 17.2 s, resulting in 4 × 4 × 5.4 mm resolution. Two rats with U87 tumor were scanned with both compressed sensing and fully sampled methods in consecutive experiments. Eight rats were scanned using the compressed sensing method only.

Data Processing and Analysis

The methods for processing ^{13}C MRSI data have been described previously (10). The raw readout data were reordered into a 4D array. Only the k-space data from flat parts of the flyback trajectory were selected. The time domain signal was apodized by a 16-Hz Gaussian filter and zero-filled to 256 points. A 4D Fourier transform was used to produce a 3D spatial array of spectra. An additional linear phase correction was applied in the flyback dimension to correct for the offset of individual k-space points (8). For the compressed sensing acquisition, an additional step after reordering into a 4D array was needed to fill in the missing k-space data due to undersampling. The missing k-space points were filled in with an iterative L_1-norm compressed sensing reconstruction. This reconstruction, described by Lustig et al. (11) and available online (http://www.eecs.berkeley.edu/~mlustig/), minimizes the L_1-norm in the wavelet domain, enforces data consistency by constraining the variation of acquired (not undersampled) k-space points, and adds a total variation penalty to promote smoothness in the spatial domains. In other words, the reconstruction is related to a nonlinear conjugate gradient algorithm for the solution of the following optimization:

$$\underset{m}{\operatorname{argmin}} |F_u(m) - y|_2 + \lambda \quad |\psi(\mathrm{m})|_1 + \alpha \mathrm{TV}(\mathrm{m}) \quad [1]$$

where three terms represent the data fidelity constraint, the L_1-norm and a total variation penalty used to enforce some edge-preserving smoothness in the final solution, respectively. The detailed description of the Eq. 1 can be found in Ref. 5. The L_1 reconstruction parameters were the same as those used in previous hyperpolarized studies, i.e., 0.0005 and 0.0001 for λ and α, respectively (5).

For quantification of ^{13}C metabolites, lactate over pyruvate ratio, lactate, pyruvate, and total carbon (tC: a sum of lactate, pyruvate-hydrate, alanine, and pyruvate) were calculated for each voxel using peak heights from magnitude spectra. The lactate, pyruvate, and tC levels were normalized to tC in blood vessels, which was obtained by taking the average of two maximum tC signals from a region outside the brain (Fig. 3). This region consistently exhibited a high level of pyruvate, which most likely originated from blood vessels, including the internal carotid artery and the vertebrobasilar arterial system that runs in the ventral surface of the brainstem. Regions of interests were manually contoured on T_1-weighted post-Gd images for contrast enhancing (CE) lesions, necrotic regions, and normal appearing brain tissue, and the percentage of each regions of interest volume was calculated for each voxel. In order to evaluate the spatial variation of ^{13}C metabolites, the median ^{13}C parameters were compared between contrast enhancement (voxels with > 65% CE lesion), necrosis (voxels with > 65% necrotic region), and normal brain (voxels with 100% normal appearing brain tissue). Statistical significance was assessed using a Wilcoxon signed-rank test or a Mann-Whitney rank-sum test.

Histopathology and Immunohistochemistry

At the end of the MR study, brains were removed and fixed in phosphate-buffered 4% formalin. Samples were then dehydrated by graded ethanols, and embedded in Paraplast Plus wax (McCormick Scientific). 5 μm sections were then examined following hematoxylin and eosin staining. Antibodies to carbonic anhydrase IX (CA9) were obtained from Novus Biologicals, Littleton Colorado and used at 1:500, 32 min/37°. Antigen retrieval for CA9 was performed for 8 min in Tris buffer (pH 8) at 90°. Immunohistochemistry was performed on the Benchmark XT (Ventana Medical Systems, Inc.) using the iView detection system. Histology and immunohistochemistry slices from the center of spectroscopic voxels were selected for comparison with ^{13}C metabolites by correlating the morphological appearance of tumor with anatomical images.

RESULTS

Figure 2 shows a T_2-weighted image, compressed sensing, and fully sampled ^{13}C MRSI data from the acetate phantom. The L_1 reconstruction for the compressed sensing design produced ^{13}C signal with excellent spectral quality. The compressed sensing data exhibited a similar spatial profile to the fully sampled data.

Figure 3 illustrates a comparison between the compressed sensing and fully sampled ^{13}C spectra acquired in consecutive scans from a rat with a brain tumor in 18.5 and 17.2 s, respectively. The factor of 3.72 acceleration in the compressed sensing scheme provided four 2 × 2 × 5.4 mm voxels (Figure 3b) for every 4 × 4 × 5.4 mm voxel in the fully sampled ^{13}C 3D echo-planar spectroscopic imaging data (Fig. 3c) in a similar acquisition time. The undersampled compressed sensing reconstructed data were in excellent agreement with the fully sampled data in terms of the overall profiles of lactate and pyruvate. The compressed sensing data revealed heterogeneous metabolic profiles within a CE lesion (light grey voxels in Figure 3b). The four voxels, which corresponded to the location of tumor, had different levels of lactate and pyruvate. Partial voluming from normal appearing brain tissue at the lower part of the spectroscopic voxel (Fig. 3a, right) resulted in low metabolic levels in two of the four voxels comprising tumor.

Compressed sensing hyperpolarized ^{13}C MRSI provided a way to evaluate the heterogeneity of metabolic profiles within brain tumor tissue. Table 1 shows the summary of ^{13}C metabolite quantification from the compressed sensing MRSI data at different radiographic regions. In all animals, lactate to pyruvate ratio, normalized lactate, pyruvate, and total carbon levels in contrast enhancement voxels (1.0 ± 0.36, 0.19 ± 0.12, 0.17 ± 0.05, and 0.40 ± 0.18, respectively) were significantly elevated compared to the respective values in normal brain voxels (0.29 ± 0.17, 0.03 ± 0.02, 0.12 ± 0.03, and 0.21 ± 0.05, respectively, $P < 0.01$). Four rats possessed necrotic voxels. Lactate to pyruvate ratio, normalized lactate and total carbon levels in these voxels (0.58 ± 0.23, 0.07 ± 0.06, and 0.21 ± 0.11, respectively) were significantly lower than those in contrast enhancement voxels ($P < 0.05$).

Figure 4 represents an example of two rats with heterogeneous tumor. Axial T_1 post-Gd images showed areas with necrosis surrounded by CE lesion in the anterior part of the brain (Fig. 4a). The voxels that corresponded to necrosis (blue voxels in Figure 4b) exhibited decreased pyruvate (0.09 ± 0.03) and negligible lactate signal (0.05 ± 0.03) in the compressed sensing ^{13}C spectra. In contrast, voxels associated with contrast enhancement (red voxels in Figure 4b) had relatively high levels of pyruvate (0.17 ± 0.05) and lactate (0.25 ± 0.25).

Figure 5 shows an example of rats with a uniform CE lesion. Axial T_1 post-Gd images displayed the uniform level of contrast enhancement across tumor tissue (Fig. 5a). The compressed sensing spectra exhibited elevated pyruvate and lactate peaks in the CE lesion (Fig. 5b). In contrast to the previous example in Figure 4, all voxels with contrast enhancement (red voxels in Figure 5b) had relatively high levels of pyruvate (0.24 ± 0.05) and lactate (0.39 ± 0.17).

The distinct metabolic patterns also correlated with different histopathologic features. Rats with heterogeneous tumor (Fig. 4) displayed areas of necrosis (blue boxes in Figure 4c) and cellular hypoxia as determined by CA9 (blue boxes in Figure 4d). Interestingly, theses necrotic and hypoxic areas corresponded to the region of ^{13}C spectra with relatively low ^{13}C metabolites (blue voxels in Figure 4b). In contrast, the sections of tumor that exhibited high levels of pyruvate and lactate signal corresponded to the area of high contrast enhancement (red voxels in Figure 4b). These regions consisted of viable tumor with minimal or no necrosis and hypoxia (red boxes in Figure 4c and d). The rats with a homogeneous level of

contrast enhancement exhibited viable tumor tissue without necrosis and with negligible hypoxia across the entire tumor volume in hematoxylin and eosin staining and CA9 slides (red boxes in Figure 5c and d). The area of viable tumor corresponded to the region of spectra with high pyruvate and lactate signal (red voxels in Figure 5b).

DISCUSSION

This study demonstrated the feasibility of evaluating heterogeneous ^{13}C metabolic profiles within brain tumor tissue in human GBM orthotopic xenografts using compressed sensing hyperpolarized 3D ^{13}C MRSI with [1-^{13}C]-pyruvate as a substrate. The improved resolution achieved by the compressed sensing scheme enabled the acquisition of heterogeneous ^{13}C metabolic profiles within tumor and made possible the differentiation between hypoxic/necrotic, nonhypoxic/necrotic tumor, and normal brain tissue (Table 1). The results from pathology confirmed that the absence or low level of pyruvate and lactate peaks was a characteristic of highly necrotic and hypoxic tissue, while tumor tissue with minimal levels of necrosis and hypoxia possessed relatively high levels of pyruvate and lactate (Figs. 4 and 5). The characterization of ^{13}C metabolites in association with variable tumor hypoxia and necrosis would be difficult at best when using conventional fully sampled echo-planar ^{13}C MRSI due to its lower resolution and the ensuing partial volume effect (Fig. 3).

Hyperpolarized ^{13}C MRSI using dynamic nuclear polarization is an emerging technique that is capable of noninvasively probing carbon metabolism with dramatically increased sensitivity. A number of recent studies have used the ^{13}C imaging of hyperpolarized [1-^{13}C]-pyruvate to study carbon metabolism in the brain (12,13). Mayer et al.(12) acquired 2D spiral ^{13}C chemical shift imaging data with in-plane resolution of 1.5×1.5 mm^2 and 5 mm slice thickness from normal rat brain using a 3T clinical system combined with a high-performance gradient insert (600 mT/m, 3200 T/m/s). Day et al.(13) acquired 2D ^{13}C chemical shift imaging data with 2.5×2.5 mm^2 in-plane resolution and 6 mm slice thickness from tumor-bearing rat brain using a 4.7T magnet designed for animal studies. In the current study, a 3T clinical system without high-performance gradient inserts was used to acquire 3D ^{13}C MRSI data with a $2 \times 2 \times 5.4$ mm^3 resolution in a brain tumor model. The use of a clinical system makes the compressed sensing method developed in this project easily translatable to future human studies.

The ^{13}C 3D flyback MRSI sequence used in this study provides a fast method for acquiring hyperpolarized spectra and is less sensitive to timing errors, eddy currents, and B_0 inhomogeneity than nonflyback versions (8). Compressed sensing in combination with a flyback readout was used to reduce acquisition time and improve spatial resolution. In order for compressed sensing to perform well, the underlying signal needs to possess sparsity and exhibit adequate signal-to-noise ratio (11). The parameters in Eq. 1 were chosen manually to balance the denoising and data fidelity constraints (6). The implementation of an automatic parameter selection scheme may be desirable in the future.

Noninvasive imaging of GBM is often complicated due to its heterogeneous and infiltrative nature (14). The ability to assess heterogeneous ^{13}C metabolic profiles with high specificity and correlate them with histopathology is of great potential for monitoring GBM progression and response to therapy. The ability to characterize distinct ^{13}C metabolic profiles using the compressed sensing method for higher spatial resolution than conventional 3D echo-planar spectroscopic imaging may assist in the noninvasive prediction of tumor tissue types and therefore, improve the management of patients with GBM.

In conclusion, we have shown that compressed sensing hyperpolarized 3D ^{13}C MRSI can provide a unique tool for quantitative evaluation of tumor metabolism and characterization

of ^{13}C metabolite patterns between hypoxic/necrotic, nonhypoxic/necrotic tumor, and normal brain tissue. Future studies will validate the findings in a larger population of animals and examine the application of this technology to patients with brain tumors.

Acknowledgments

The authors gratefully acknowledge the assistance of Dr. Michael Lustig for advice on implementing the compressed sensing methods, and Peter Shin and Llewelyn Jalbert for processing data and assisting in experiments.

Grant sponsor: American Brain Tumor Association (basic research fellowship to I. Park); Grant sponsor: NIH; Grant numbers: R01EB007588, P41EB13598; Grant sponsor: University of California and GE Healthcare; Grant number: ITL-BIO04-10148 (academic-industry partnership).

REFERENCES

1. Ardenkjaer-Larsen JH, Fridlund B, Gram A, Hansson G, Hansson L, Lerche MH, Servin R, Thaning M, Golman K. Increase in signal-to-noise ratio of >10,000 times in liquid-state NMR. Proc Natl Acad Sci USA. 2003; 100:10158–10163. [PubMed: 12930897]
2. Park I, Larson PE, Zierhut ML, et al. Hyperpolarized 13C magnetic resonance metabolic imaging: application to brain tumors. Neuro Oncol. 2010; 12:133–144. [PubMed: 20150380]
3. Park I, Bok R, Ozawa T, Phillips JJ, James CD, Vigneron DB, Ronen SM, Nelson SJ. Detection of early response to temozolomide treatment in brain tumors using hyperpolarized 13C MR metabolic imaging. J Magn Reson Imaging. 2011; 33:1284–1290. [PubMed: 21590996]
4. Chaumeil MM, Ozawa T, Park I, Scott K, James CD, Nelson SJ, Ronen SM. Hyperpolarized (13)C MR spectroscopic imaging can be used to monitor Everolimus treatment in vivo in an orthotopic rodent model of glioblastoma. Neuroimage. 2012; 59:193–201. [PubMed: 21807103]
5. Hu S, Lustig M, Balakrishnan A, et al. 3D compressed sensing for highly accelerated hyperpolarized 13C MRSI with in vivo applications to transgenic mouse models of cancer. Magn Reson Med. 2010; 63:312–321. [PubMed: 20017160]
6. Hu S, Lustig M, Chen AP, et al. Compressed sensing for resolution enhancement of hyperpolarized 13C flyback 3D-MRSI. J Magn Reson. 2008; 192:258–264. [PubMed: 18367420]
7. Derby K, Tropp J, Hawryszko C. Design and evaluation of a novel dual-tuned resonator for spectroscopic imaging. J Magn Reson. 1990; 86:645–651.
8. Cunningham CH, Vigneron DB, Chen AP, Xu D, Nelson SJ, Hurd RE, Kelley DA, Pauly JM. Design of flyback echo-planar readout gradients for magnetic resonance spectroscopic imaging. Magn Reson Med. 2005; 54:1286–1289. [PubMed: 16187273]
9. Cunningham CH, Chen AP, Albers MJ, Kurhanewicz J, Hurd RE, Yen YF, Pauly JM, Nelson SJ, Vigneron DB. Double spin-echo sequence for rapid spectroscopic imaging of hyperpolarized 13C. J Magn Reson. 2007; 187:357–362. [PubMed: 17562376]
10. Nelson SJ. Analysis of volume MRI and MR spectroscopic imaging data for the evaluation of patients with brain tumors. Magn Reson Med. 2001; 46:228–239. [PubMed: 11477625]
11. Lustig M, Donoho D, Pauly JM. Sparse MRI: the application of compressed sensing for rapid MR imaging. Magn Reson Med. 2007; 58:1182–1195. [PubMed: 17969013]
12. Mayer D, Yen YF, Takahashi A, Josan S, Tropp J, Rutt BK, Hurd RE, Spielman DM. Dynamic and high-resolution metabolic imaging of hyperpolarized [1–13C]-pyruvate in the rat brain using a high-performance gradient insert. Magn Reson Med. 2011; 65:1228–1233. [PubMed: 21500253]
13. Day SE, Kettunen MI, Cherukuri MK, Mitchell JB, Lizak MJ, Morris HD, Matsumoto S, Koretsky AP, Brindle KM. Detecting response of rat C6 glioma tumors to radiotherapy using hyperpolarized [1-13C]pyruvate and 13C magnetic resonance spectroscopic imaging. Magn Reson Med. 2011; 65:557–563. [PubMed: 21264939]
14. Bohman LE, Swanson KR, Moore JL, Rockne R, Mandigo C, Hankinson T, Assanah M, Canoll P, Bruce JN. Magnetic resonance imaging characteristics of glioblastoma multiforme: implications for understanding glioma ontogeny. Neurosurgery. 2010; 67:1319–1327. [PubMed: 20871424]

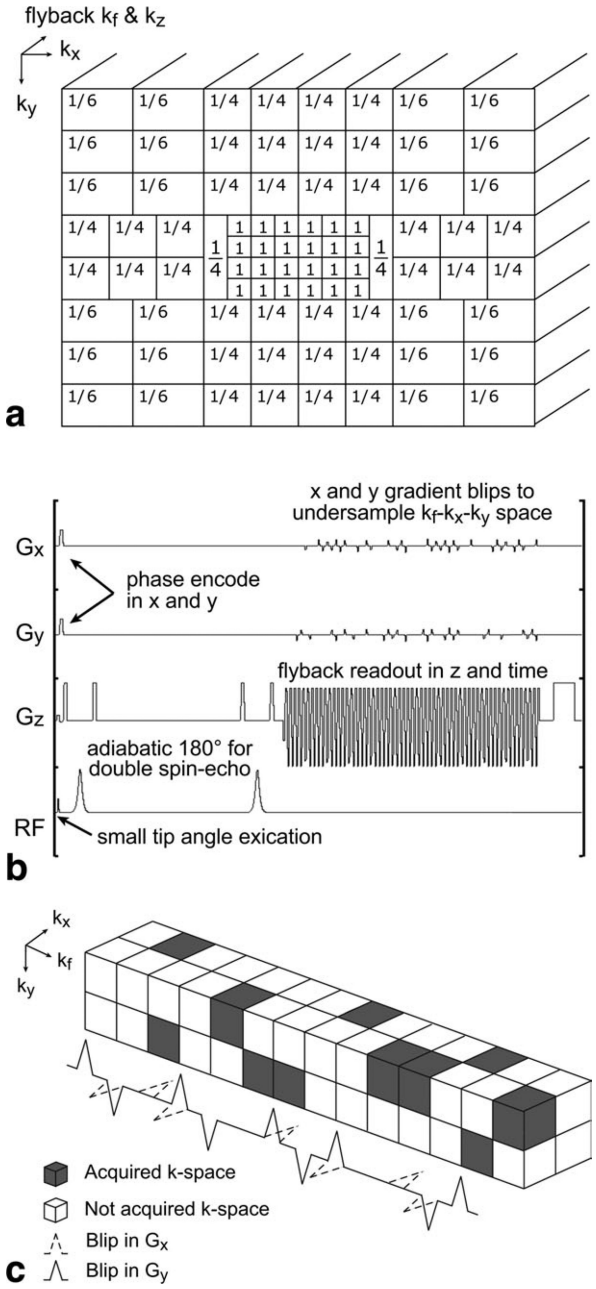

FIG. 1.

An undersampling pattern for the new compressed sensing scheme (a) and pulse sequence timing diagram for compressed sensing ^{13}C MRSI (b). The numbers in (a) represent the fraction of samples collected in each k_x-k_y-k_f block. c: Illustration of random undersampling in k_x-k_y-k_f space. Random undersampling was achieved by implementing blips in the x and y gradients.

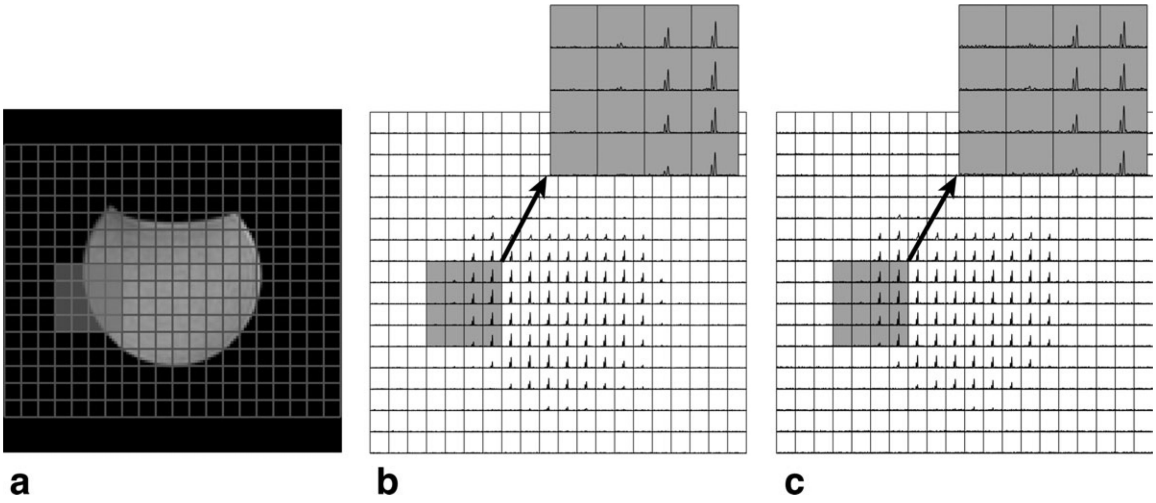

FIG. 2.

An anatomical image of a phantom (a) and ^{13}C spectra acquired using the new compressed sensing design (b) and fully sampled method (c). The compressed sensing reconstructed data produced ^{13}C acetate signal with high spectral quality and matched the fully sampled data.

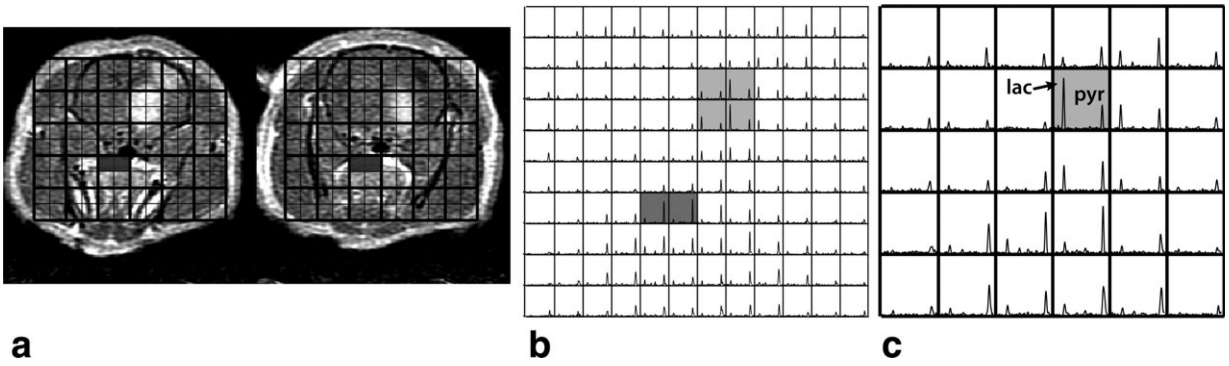

FIG. 3.

Compressed sensing (b) and fully sampled (c) ^{13}C 3D MRSI data acquired in successive scans. T_1 post-Gd images corresponding to the location of ^{13}C spectra are shown in (a). The overall profiles of pyruvate and lactate were consistent between the two methods. The light grey voxels represent ^{13}C spectra from tumor tissue. The dark grey voxels contained high pyruvate signal from blood vessels, which were used to normalize lactate, pyruvate, and total carbon levels.

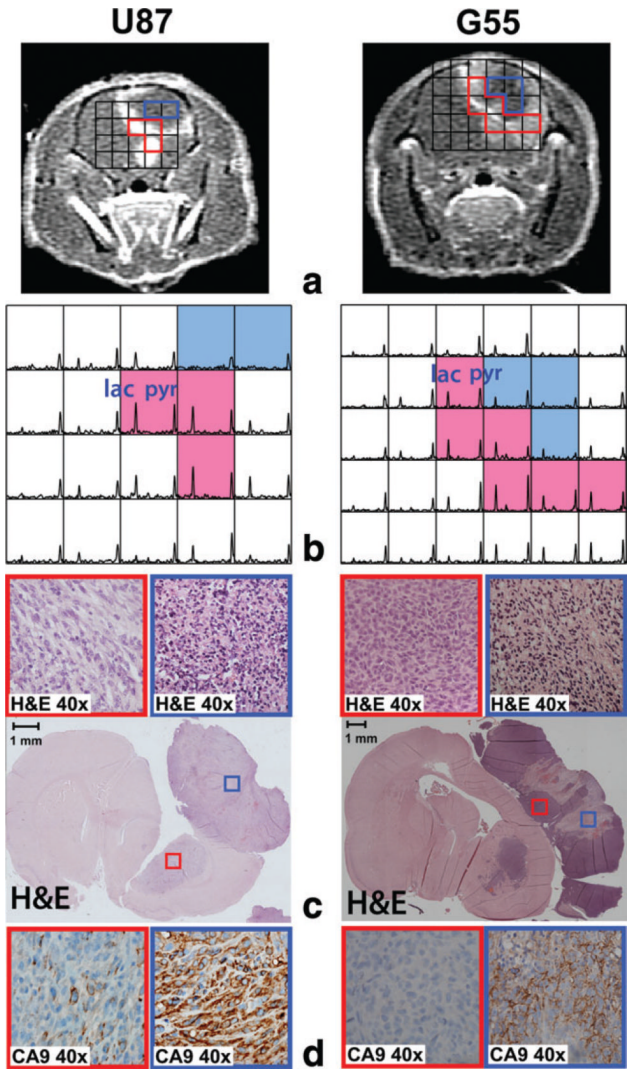

FIG. 4.

An example of two rats with heterogeneous tumors showing T_1 post-Gd images (a), ^{13}C spectra (b) and histopathology (c, d). The voxels representing necrosis (blue voxels in b) and contrast enhancement (red voxels in b) exhibited distinct ^{13}C metabolic profiles from the compressed sensing data. Hematoxylin and eosin staining and CA9 immunostaining demonstrated substantial necrosis and hypoxia (blue boxes in c and d) in the area with small pyruvate and lactate (blue voxels in b) while the area with high ^{13}C metabolites (red voxels in b) consisted of viable tumor with minimal or no necrosis and hypoxia (red boxes in c and d).

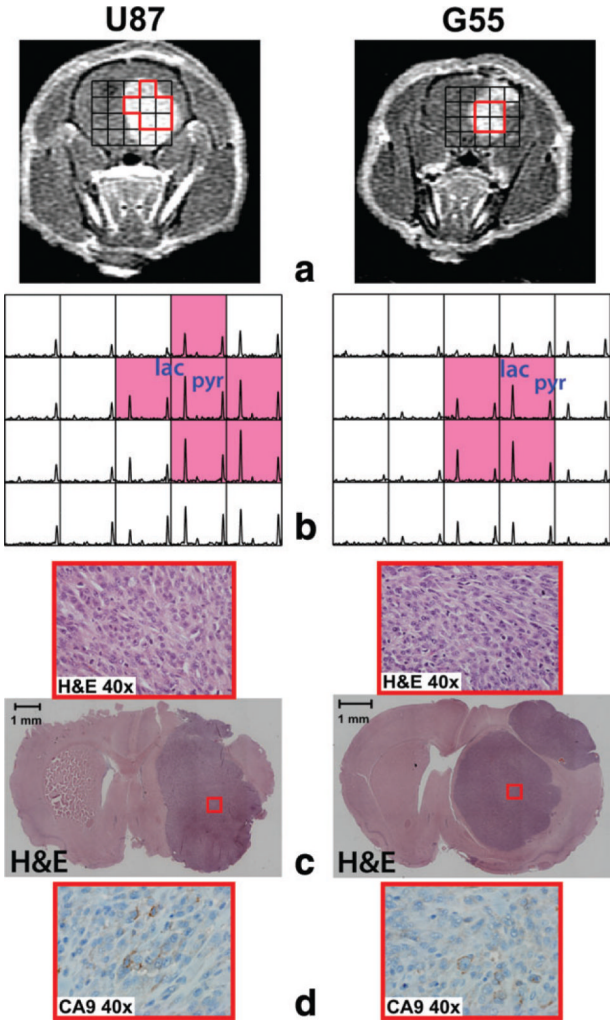

FIG. 5.

An example of two rats with a uniform CE lesion showing T_1 post-Gd images (a), ^{13}C spectra (b), and histopathology (c, d). Compressed sensing ^{13}C spectra displayed highly elevated pyruvate and lactate consistently across the contrast enhancement voxel (red voxels in b). The corresponding hematoxylin and eosin staining and CA9 slides showed viable tumor without substantial necrosis and hypoxia (red boxes in c and d).

Table 1

Summary of ^{13}C metabolite Quantification at Different Radiographic Voxels

	Lac/Pyr[a,b]	Lac[a,b]	Pyr[a]	tC[a,b]
Normal brain (n = 10)	0.29 ± 0.17	0.03 ± 0.02	0.12 ± 0.03	0.21 ± 0.05
Contrast enhancement (n = 10)	1.0 ± 0.36	0.19 ± 0.12	0.17 ± 0.05	0.40 ± 0.18
Necrosis (n = 4)	0.58 ± 0.23	0.07 ± 0.06	0.11 ± 0.05	0.21 ± 0.11

Lac/Pyr represents the lactate over pyruvate ratio. Lac, Pyr and tC represent the lactate, pyruvate, and total carbon levels normalized by vascular total carbon signal. All values are reported as median ± SD.

[a] Significant difference between normal brain and contrast enhancement ($P < 0.01$, Wilcoxon signed-rank test).

[b] Significant difference between contrast enhancement and necrosis ($P < 0.05$, Mann-Whitney rank-sum test).